Supplement

Beyond stomata: Interspecific heterogeneity and structural controls of urban ozone deposition

Wen Dong [1], Xingbao Wang [1], Kai Xu, Hanxing Zhou, Yincheng Huang, Zhi Lou, Yue Zhang, Zhenyang Huang, Jing Zhang, Junjiong Shao, Yuanyuan Du, Xiaoai Jin, Jian Chen, and Yuan Ren *

[1]These authors contributed equally to this work.

A summary of this file

The number of pages: 14

The number of additional Sections: 4

The number of Tables: 1

The number of Figures: 6

Text S1. The relationship between leaf area density and tree height

To accurately simulate the turbulent transport mechanisms within the canopy and the vertical deposition flux of ozone, this study simplifies the crown structure into four idealized geometric shapes based on the growth characteristics of common urban greening tree species: conical, umbrella, round, and cylindrical. The vertical distribution of leaf area density (*LAD*) with height (z) directly determines the calculation accuracy of the within-canopy momentum transfer coefficient (K_m) and the aerodynamic resistance (R_a).

As shown in Fig. S1-S4, the vertical *LAD* profiles corresponding to different crown shapes exhibit marked differences. The conical crown concentrates *LAD* mainly in the middle and lower parts of the canopy, decreasing linearly or nonlinearly with increasing height, which reflects the typical characteristics of certain pyramid-shaped broadleaf trees. The umbrella crown has a *LAD* peak clearly biased toward the top of the canopy, with a distribution pattern resembling that of tall broadleaf forests; this structure causes the majority of ozone uptake to occur in the active leaf layer at the canopy top. The round crown shows a relatively symmetrical leaf distribution, with the *LAD* peak typically occurring at the mid-height of the crown, making it suitable for simulating most uniformly branched urban shade tree species. The cylindrical crown maintains a relatively uniform *LAD* distribution over the entire crown height, representing neatly trimmed hedges or specific landscape tree species with vertical growth. The choice of these vertical profiles is critical for the MGM model, because an unrealistic *LAD* profile may lead to errors in the estimated V_d by up to a factor of two.

Text S2. Schematics of in-situ observation systems for selected tree species

This section presents, through field observation photographs (Fig. S5), a detailed view of the in-situ experimental setup supporting the calculations of the modified micrometeorological gradient method (MGM). To enable accurate monitoring of 20 representative urban greening tree species in the complex urban habitat of Hangzhou, a mobile elevated observation platform was developed and deployed, with its vertical sampling height dynamically adjustable within a 14 m range according to the growth height of each tree species. As shown in Fig. S5, the observation system achieves vertically stratified monitoring of O_3 concentration via a precisely designed sensor mast. Sampling points are arranged strictly following the requirements of the MGM model at three key levels: above-canopy (z_1), canopy-top (h), and within-canopy (z_2). Each level is connected to a high-precision UV photometric ozone analyzer (Thermo Scientific 49i) to ensure that the weak but critical vertical concentration gradients can be captured.

Furthermore, the aluminum alloy scaffolding platform shown in the photographs not only provides a stable base for sensors such as the three-dimensional sonic anemometer and thermo-hygrometer, but also minimizes the disturbance of the platform itself to the turbulence field above the canopy by optimizing the horizontal spacing. This in-situ configuration ensures the spatial representativeness of the acquired data, thereby providing realistic and reliable physical boundary conditions for the resistance partitioning and V_d estimation described in Text S3.

Text S3. Calculation of ozone dry deposition

This section describes the mathematical framework and parameterization scheme used to estimate the dry deposition flux of ozone (O_3). Because traditional micrometeorological gradient methods, such as the aerodynamic gradient method (AGM) and the modified Bowen ratio (MBR), measure extremely small concentration gradients above the forest canopy, they often introduce substantial uncertainties into the calculated fluxes. To address this issue, this study adopts the modified micrometeorological gradient method (MGM) proposed by Wu et al. (2015). The MGM estimates the flux using the concentration gradient between the canopy top and the layers below, combined with within-canopy turbulence characteristics such as the leaf area density (*LAD*) profile and the wind speed attenuation coefficient.

In calculating the dry deposition velocity (V_d) and deriving the canopy resistance (R_c), this study strictly follows the classical three-resistance analogy model introduced by Zhang et al. (2003). Based on an analogy with Ohm's law, the model parameterizes the processes of atmospheric transport and surface uptake as a series combination of the aerodynamic resistance (R_a), the quasi-laminar sublayer resistance (R_b), and the bulk canopy resistance (R_c). The canopy resistance (R_c) is further partitioned into parallel stomatal (R_s and mesophyll resistance R_m) and non-stomatal (R_{ns}) pathways; the latter encompasses cuticular uptake, in-canopy aerodynamic transport, and soil uptake. By incorporating meteorological and biological factors such as friction velocity, relative humidity (*RH*), and leaf area index (*LAI*), the revised parameterization scheme markedly improves model accuracy over various underlying surfaces, particularly under wet-canopy conditions. The subsequent equations (Eqs. 1–17) provide a detailed derivation of the flux within the MGM framework and specify the computational procedures for each resistance component based on the three-resistance analogy model.

Assuming that atmospheric turbulence can be treated as a molecular diffusion process (Baldocchi, 1988), the flux-gradient theory can be expressed simply as:

$$F(z) = -K_c(z)\frac{dC}{dz} \quad (1)$$

where $K_c(z)$ the vertical eddy diffusivity, and dC/dz is the vertical concentration gradient of the gas. K_c is related to the aerodynamic resistance (R_a) of the air layer by：

$$Ra(z_1:h) = \int_h^{z_1} \frac{dz}{K_c}(z) \quad (2)$$

where z_1 and h denote the heights of the canopy top and the adjacent layer above, respectively ($z_1>h$). Combining Eqs. (1) and (5), the deposition flux (F) can be expressed as：

$$\mathrm{F} = -\frac{\triangle \mathrm{C}}{Ra(z_1:h)} = -\frac{\mathrm{C_1} - \mathrm{C_h}}{Ra(z_1:h)} \quad (3)$$

where C_1 and C_h are the gas concentrations at heights z_1 and h, respectively. The aerodynamic resistance $R_a(z_1 : h)$ is calculated as:

$$R_a(z_1:h) = (ku_*)^{-1}\left[ln\frac{z_1-d}{h-d} + \Psi_h\left(\frac{z_1-d}{L}\right) - \Psi_h\left(\frac{h-d}{L}\right)\right] \quad (4)$$

where k is the von Kármán constant (0.4), $u*$ is the friction velocity measured at the reference height, d is the zero-plane displacement height, L is the Obukhov length, and Ψ_h is the integrated stability correction function for heat, based on Businger et al. (1971) as revised by Högström (1988). According to Eq. (1), the O_3 flux at the canopy top F(h) is defined as:

$$F(h) = -\frac{C_h - C_2}{R_a(h:z_2)} \quad (5)$$

where C_h and C_2 are the concentrations at the canopy top (h) and at height z_2 ($z_2<h$), respectively. $Ra(h : z_2)$ is related to K_c by:

$$Ra(h:z_2) = \int_{z_2}^{h} \frac{dz}{K_c}(z) \quad (6)$$

Based on the assumption of a constant flux layer above the canopy, the O_3 flux above the canopy obtained from Eq. (6) should equal the O_3 flux at the canopy top given by Eq. (3). From Eqs. (3) and (6) we can derive:

$$F = -\frac{C_1 - C_2}{R_a(z_1 : h) + R_a(h : z_3)} \quad (7)$$

$R_a(z_1:h)$ is computed using Eq. (4), and $R_a(h:z_2)$ is obtained by vertical integration of Eq. (4) between the two heights within the canopy. It is assumed that $K_c(z)$ equals 0.8 $K_m(z)$, where $Km(z)$ is the eddy diffusivity for momentum transfer within the canopy. $Km(z)$ is determined as:

$$\mathrm{K_m(z)} = \frac{\int_0^z C_m(z)a(z)u(z)^2 dz}{du(z)/dz} \quad (8)$$

where $a(z)$ is the leaf area density at height z, and $u(z)$ is the horizontal wind speed within the canopy. It is assumed that $K_m(z)$ is constant below the canopy closure (approximately 0.7 h) and equals $K_m(z)$ at 0.7 h. The effective drag coefficient $C_m(z)$ is assumed to be invariant with height:

$$\mathrm{C_m(z)} = \frac{C_{am}}{LAI[u_m/u(z_1)]^2} \quad (9)$$

where LAI is the canopy leaf area index, u_m is the mean wind speed within the canopy, and $u(z_1)$ is the wind speed at the reference height z_1. The canopy drag coefficient (C_{am}) is calculated as:

$$C_{am} = \frac{u_*^2}{uu(z_1)^2} \quad (10)$$

The mean within-canopy wind speed (u_m) is calculated as:

$$u_m = (1/h)\int_0^h u(z)dz \quad (11)$$

The within-canopy wind speed profile $u(z)$ is given by:

$$u(z) = u_h e^{-\alpha(1-z/h)} \quad (12)$$

where u_h is the wind speed at the canopy top, and α is the wind speed attenuation coefficient. Using the logarithmic wind profile above the canopy, the wind speed measured at the reference height z_1 is converted to the canopy height h:

$$u_h = u(z_1)\frac{\ln(h-d) - \ln(z_0) + \Psi_m\left[\frac{h-d}{L}\right] - \Psi_m\left[\frac{z_0}{L}\right]}{\ln(z_1-d) - \ln(z_0) + \Psi_m\left[\frac{z_1-d}{L}\right] - \Psi_m\left[\frac{z_0}{L}\right]} \quad (13)$$

where z_0 is the roughness length for momentum. Assuming the concentration at the absorbing surface is zero, the dry deposition velocity of O_3 (V_d) is defined as

$$V_d = -F/C_1 \quad (14)$$

where C_1 is the O_3 concentration measured at the reference height z_1.

The computation of V_d requires the aerodynamic resistance (R_a) and the quasi-laminar boundary layer resistance (R_b) to be determined using standard micrometeorological theory. R_a is calculated via the Monin–Obukhov similarity theory (MOST) (Zhang et al., 2003), and R_b is estimated based on the friction velocity and the ratio of the molecular diffusivities of momentum and the trace gas (O_3) (Zhang et al., 2003). The environmentally sensitive canopy resistance (R_c) is subsequently derived from the three-resistance analogy model:

$$R_c = V_d^{-1} - R_a - R_b \quad (15)$$

R_a is obtained from Eqs. (4) and (6), and the quasi-laminar boundary layer resistance R_b is calculated as:

$$R_b = 2.2(v/D_a)^{2/3}(ku^*)^{-1} \quad (16)$$

where v is the kinematic viscosity of air ($1.505 \times 10^{-5} m^2\ s^{-1}$). D_a is the molecular diffusivity of O_3 in air, calculated as:

$$D_a = \frac{0.143 * T^{1.75}\sqrt{\frac{1}{2}\left(\left(\frac{1}{M_a} + \frac{1}{M}\right)\right)}}{P[(\sum V)_a^{0.33} + (\sum V)^{0.33}]^2} \quad (17)$$

where P is the total atmospheric pressure (Pa), M_a is the molecular weight of air (28.966 g mol^{-1}), M is the molecular weight of the compound (for O_3, 48 g mol^{-1}), $(\sum V)$a is the molecular volume of air (19.7), and $\sum V$ is the molecular diffusion volume (typically 48 $cm^3\ mol^{-1}$).

Text S4. Resistance-based inversion of species-specific stomatal and non-stomatal parameters

To reduce the influence of short-term environmental variability on interspecific comparison (Wesely et al., 2002), the observed apparent canopy resistance was further decomposed into stomatal resistance (R_s) and non-stomatal resistance (R_{ns}) using a parallel-resistance framework:

$$R_c^{-1} = R_s^{-1} + R_{ns}^{-1} \tag{18}$$

R_s was expressed as a function of a minimum stomatal resistance ($R_{s,min}$) parameter and environmental response functions:

$$R_s(t) = R_{s,min}[f_1(t) \cdot f_2(t) \cdot f_3(t) \cdot f_4(t)]^{-1} \tag{19}$$

Because continuous soil-moisture observations were unavailable in the present study, the soil-moisture limitation term was set to a constant value of f_2=1. The remaining environmental response functions were defined as:

$$f_1(t) = \left(\frac{G(t)}{G_r} + 0.01\right)\left(\frac{G(t)}{G_r} + 1\right)^{-1} \tag{20}$$

$$f_2(t) = 1 \tag{21}$$

$$f_3(t) = (1 + \alpha\delta e(t))^{-1} \tag{22}$$

$$f_4(t) = max[0, 1 - 0.0016(298.0 - T_a(t))^2] \tag{23}$$

where $G(t)$ is solar irradiance, G_r is the reference irradiance, $\delta e(t)$ is vapor pressure deficit (kPa), $T_a(t)$ is air temperature (K), and α is the response coefficient for vapor pressure deficit. The combined environmental constraint term was therefore:

$$f_{env}(t) = f_1(t) \cdot f_2(t) \cdot f_3(t) \cdot f_4(t) \tag{24}$$

The modeled canopy resistance was then expressed as:

$$R_{c,mod}(t) = \left[R_s(t)^{-1} + {R_{ns}}^{-1}\right]^{-1} \tag{25}$$

For each species, $R_{s,min}$ and R_{ns} were estimated from the full diurnal time series

using nonlinear least-squares fitting, such that the modeled canopy resistance $R_{c,mod}(t)$ best matched the observed canopy resistance $R_{c,obs}(t)$. The objective function was:

$$\min \sum_{t} \left[R_{c,obs}(t) - R_{c,mod}(t)\right]^2 \quad (26)$$

Only daytime periods with positive irradiance were used in this inversion step. During optimization, both $R_{s,min}$ and R_{ns} were constrained to positive values.

References

Baldocchi, D.: A multi-layer model for estimating sulfur dioxide deposition to a deciduous oak forest canopy, Atmos. Environ., 22, 869–884, https://doi.org/10.1016/0004-6981(88)90264-8, 1988.

Businger, J. A., Wyngaard, J. C., Izumi, Y., and Bradley, E. F.: Flux-profile relationships in the atmospheric surface layer, J. Atmos. Sci., 28, 181–189, https://doi.org/10.1175/1520-0469(1971)028<0181:FPRITA>2.0.CO;2, 1971.

Högström, U.: Non-dimensional wind and temperature profiles in the atmospheric surface layer: a re-evaluation, Boundary-Layer Meteorol., 42, 55–78, https://doi.org/10.1007/BF00119875, 1988.

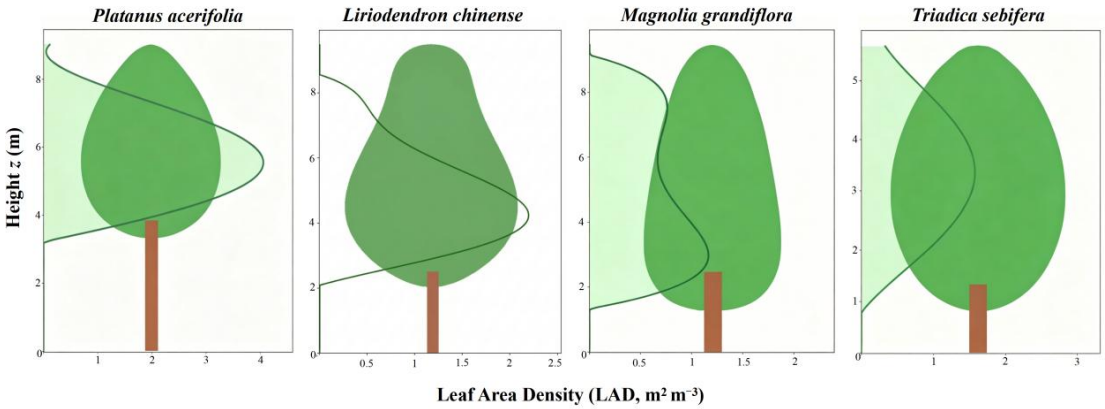
Wesely, M. L., Doskey, P. V., and Shannon, J. D.: Deposition parameterizations for the Industrial Source Complex (ISC3) model, ANL/ER/TR-01/003, Argonne National Laboratory, Environmental Research Division, Argonne, IL, USA, 128 pp., 2002.

Wu, Z. Y., Zhang, L., Wang, X. M., et al.: A modified micrometeorological gradient method for estimating O3 dry depositions over a forest canopy, Atmos. Chem. Phys., 15, 7487–7496, https://doi.org/10.5194/acp-15-7487-2015, 2015.

Zhang, L., Brook, J. R., and Vet, R.: A revised parameterization for gaseous dry deposition in air-quality models, Atmos. Chem. Phys., 3, 2067–2082, https://doi.org/10.5194/acp-3-2067-2003, 2003.

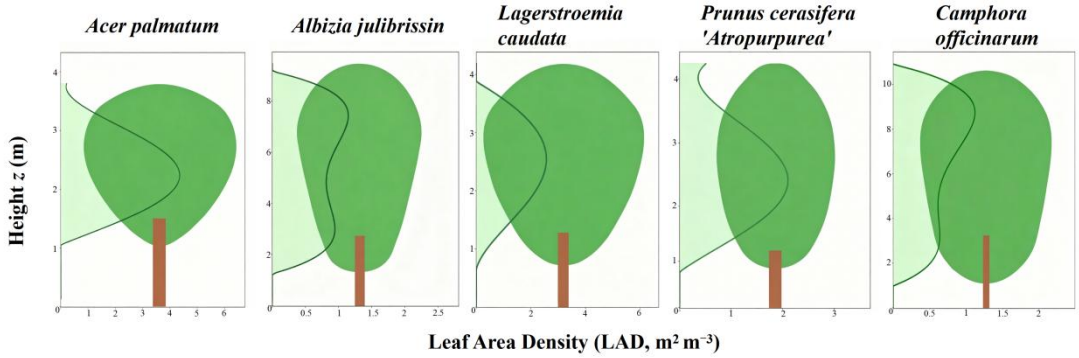
Table S1. Dendrometric characteristics and functional classifications of the 20 studied urban tree species. Values are presented as species-level means ± standard error derived from three independent biological replicates (n = 3).

Latin name	PFT	Tree height (m)	DBH (cm)	Crown width (m)
Osmanthus fragrans	ebt	4.48±0.35	21.98±1.54	2.50±0.22
Sophora japonica L	dbt	3.28±0.28	21.8±1.65	1.25±0.18
Lagerstroemia caudata	dbt	4.35±0.38	33.44±2.81	2.32±0.25
Triadica sebifera	dbt	5.81±0.52	18.25±1.34	2.41±0.32
Albizia julibrissin	dbt	9.11±0.85	25.48±2.12	5.56±0.68
Camphora officinarum	ebt	10.91±1.02	43.95±3.56	7.25±0.94
Acer palmatum	dbt	3.65±0.31	17.2±1.28	2.49±0.35
Liriodendron chinense	dbt	9.96±0.92	27.39±2.45	3.65±0.48
Ginkgo biloba	dbt	8.35±0.74	25.52±2.08	2.48±0.31
Quercus glauca	ebt	8.35±0.68	29.3±2.34	4.32±0.52
Magnolia grandiflora	ebt	9.45±0.81	25.48±1.95	3.15±0.39
Pinus massoniana	ent	5.22±0.46	26.43±2.18	2.55±0.34
Photinia serratifolia	ebt	4.12±0.33	16.82±1.41	1.69±0.21
Prunus cerasifera 'Atropurpurea'	dbt	4.32±0.37	13.25±1.15	2.69±0.38
Prunus serrulata	dbt	3.36±0.29	18.92±1.52	2.18±0.27
Morella rubra	ebt	4.68±0.42	19.1±1.63	2.98±0.41
Prunus serrulate var. *lannesiana*	dbt	3.56±0.31	23.95±1.88	2.91±0.36
Michelia chapensis	ebt	7.95±0.65	21.34±1.76	2.75±0.32
Liquidambar formosana	dbt	6.95±0.58	21.82±1.92	2.65±0.34
Platanus acerifolia	dbt	9.01±0.82	18.15±1.57	3.01±0.43



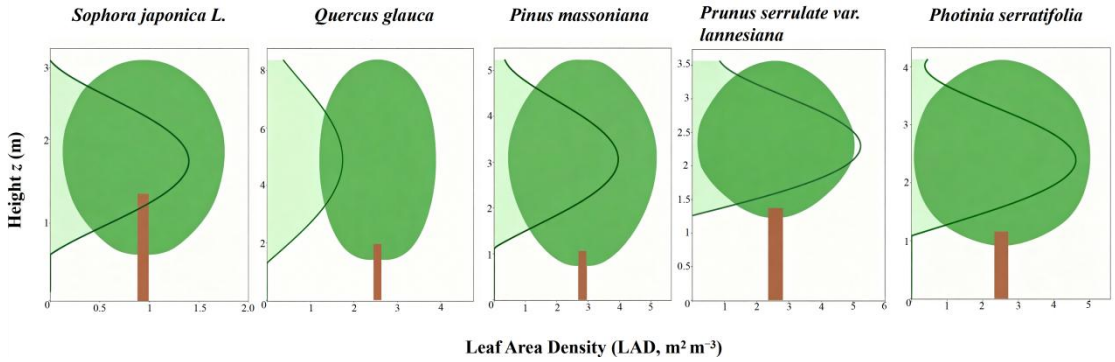
210

211 **Figure S1.** Vertical distribution characteristics of leaf area density (LAD) decreasing along
212 relative tree height in an idealized conical crown



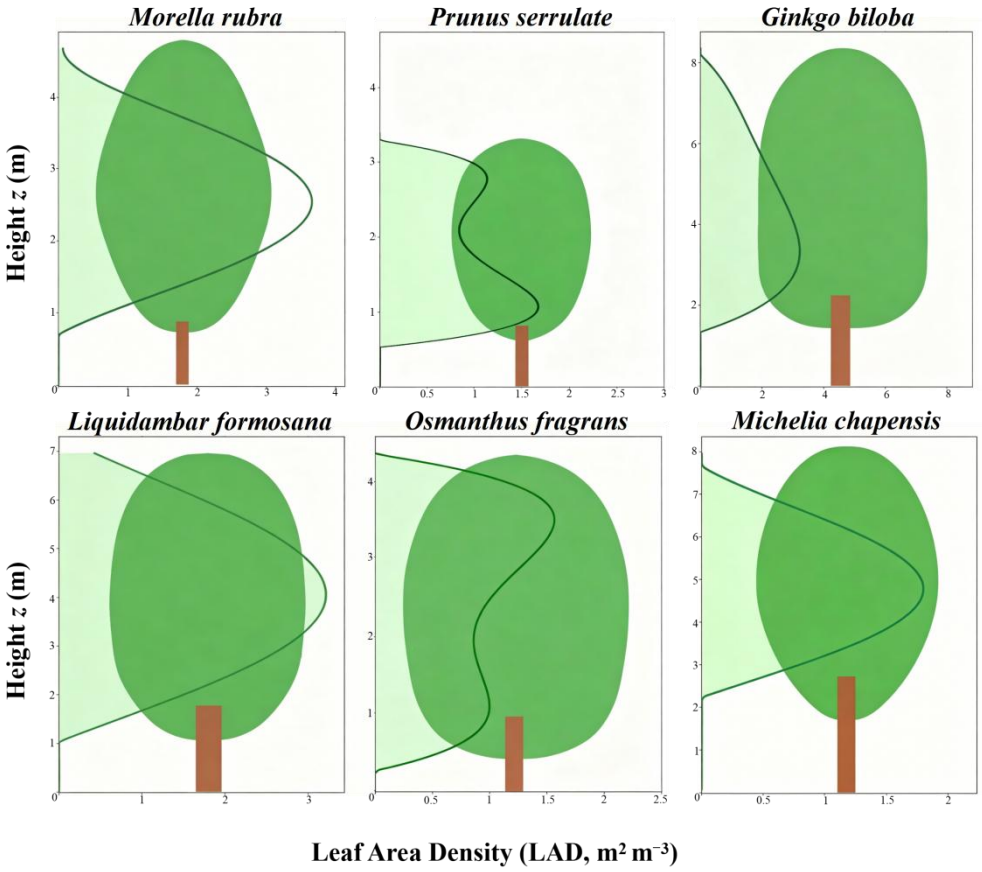
213

214 **Figure S2.** Vertical distribution characteristics of leaf area density (LAD) concentrated in the
215 upper canopy of an idealized umbrella-shaped crown
216



217

218 **Figure S3.** Vertical distribution characteristics of leaf area density (LAD) with a symmetric
219 pattern peaking in the middle canopy of an idealized spherical crown



220

221 **Figure S4.** Vertical distribution characteristics of leaf area density (LAD) uniformly distributed

222 along canopy height in an idealized cylindrical crown

223

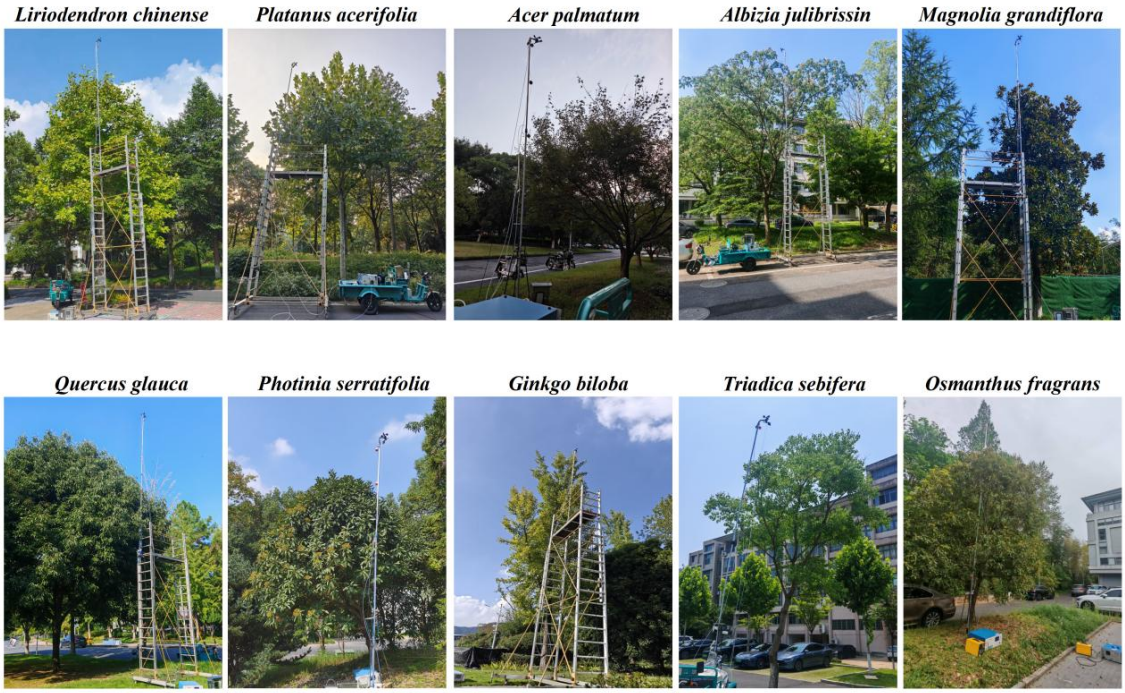


Figure S5. Photographs of the in-situ experimental configurations and mobile observation platforms used for measuring ozone dry deposition fluxes of representative urban tree species in Hangzhou, China. The monitoring systems feature height-adjustable sampling masts and 3D ultrasonic anemometers positioned to capture vertical ozone concentration gradients and micrometeorological parameters. Sampling inlets were strategically placed at three key vertical levels—above-canopy reference height (z_1), canopy-top (h), and within-canopy active layer (z_2)—to satisfy the requirements of the Modified Micrometeorological Gradient Method (MGM).

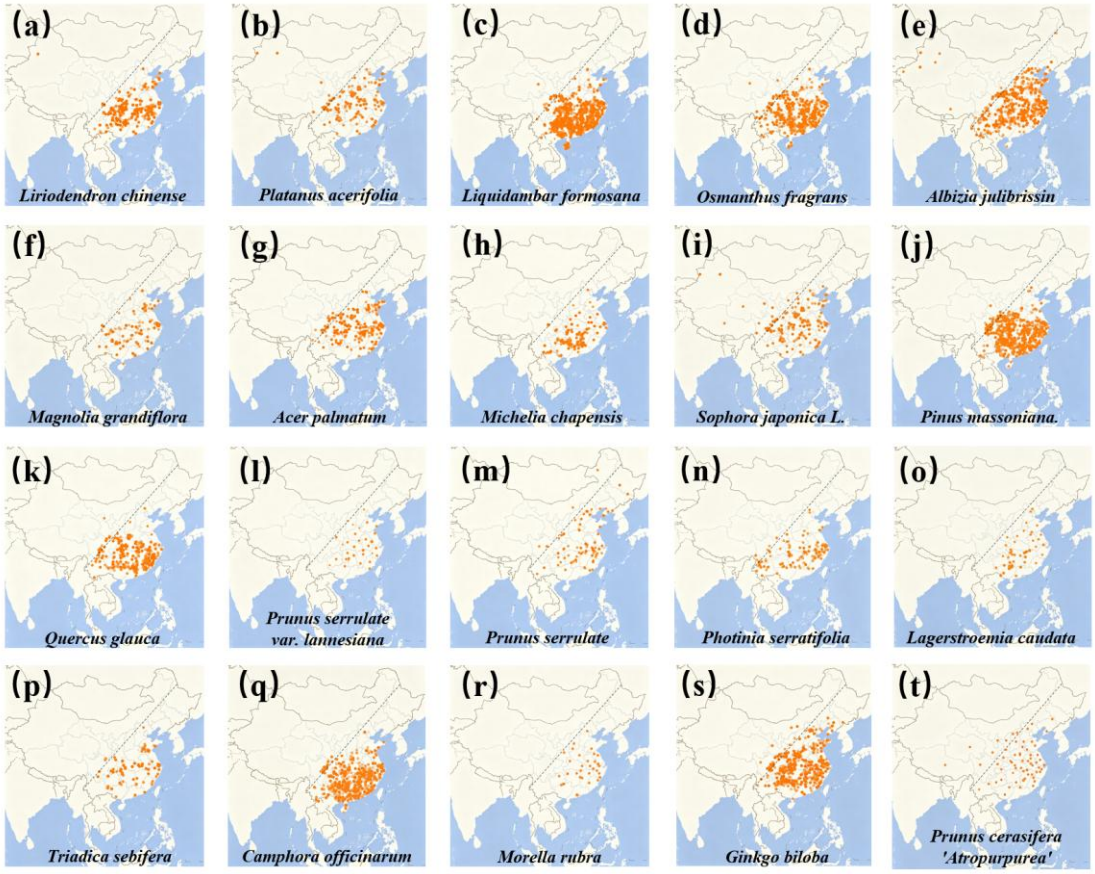


Figure S6. Species geographic distribution maps across China indicating regional and global generalizability under urban biotic homogenization. The panels (a – t) illustrate the extensive geographical ranges of the 20 investigated urban greening tree species. The dashed lines denote the Hu Line (Heihe–Tengchong Line), a major demographic and biogeographical boundary east of which accommodates over 94% of China's population and the vast majority of its built-up urban agglomerations. Driven by urban biotic homogenization, these 20 species constitute the dominant canopy framework across broad climatic zones: *Camphora officinarum* serves as the core evergreen species throughout the massive Yangtze River Basin, *Styphnolobium japonicum* serves as the standard baseline row-tree for northern temperate cities, and *Ginkgo biloba* is ubiquitously cultivated nationwide. Crucially, key taxa such as *Platanus acerifolia* and *Magnolia grandiflora* represent the most ubiquitous street trees globally, widely utilized across North American and European megacities. Their wide distribution across diverse macroclimatic conditions ensures that the derived species-resolved ozone resistance parameterizations are not confined to a narrow ecological niche, but possess robust transferability to global urban air-quality models.